Restoration of Multichannel Microwave Radiometric Images

Roland T. Chin,* Chia-Lung Yeh,* and William S. Olson**

*Department of Electrical and Computer Engineering
** Department of Meteorology
University of Wisconsin-Madison
Madison, Wisconsin 53706

ABSTRACT

A constrained iterative image restoration method is applied to multichannel diffraction-limited imagery. This method is based on the Gerchberg-Papoulis algorithm utilizing incomplete information and partial constraints. The procedure is described using the orthogonal projection operators which project onto two prescribed subspaces iteratively. Some of its properties and limitations are also presented. The selection of apropriate constraints was emphasized in a practical application. Multichannel microwave images, each having different spatial resolution, were restored to a common highest resolution to demonstrate the effectiveness of the method. Both noise-free and noisy images were used in this investigation.

Index Terms - Digital Image Restoration, Superresolution, Constrained Iterative Restoration, Multichannel Diffraction-Limited Imagery, Microwave Radiometers.

This work was supported in part by the National Aeronautics and Space Administration (NASA) under Grant No. NAGW-380 and by the University of Wisconsin-Madison, Wisconsin Alumni Research Foundation (WARF) under Grant No. 130408.

Presented at the Computer Vision and Pattern Recognition Conference, June 19-23, 1983, Arlington, VA. Also submitted to the IEEE Trans. Pattern Analysis and Machine Intelligence.

1. Background

Multichannel microwave radiometers on the Seasat and Nimbus 7 satellites offer a quantitative method for measuring geophysical parameters over the ocean. The emissivity of the ocean surface is low and varies predictably with wind speed; it thus provides a good background for observing precipitation. The theory and initial validation of this concept was given by Wilheit, et al. [1].

Recently Olson [2] employed a radiative transfer model to simulate the polarized brightness temperatures that a Scanning Multichannel Microwave Radiometer (SMMR) would measure from hurricanes over sea surfaces at several frequencies (6.6, 10.7, 18.0, 21.0, and 37.0 GHz each with two polarizations). These brightness temperatures depend upon the rainfall rates, rain column height, and the emissivity of the wind roughened sea surface. It became evident that the 37 GHz channel is most sensitive to the height of the freezing level, whereas the 10.7 or 18 GHz channels are sensitive to changes in rainfall rates when those rates are less than 10 to 20 mm/hr. The 6.6 GHz channel provides rain information when the rainfall rate exceeds these values. The information content of each channel is a variable function of rainfall rate, rain column height, and emissivity of the sea surface, and the dependencies are generally nonlinear. A piecewise-linear regression algorithm has been applied to the synthetic data in the manner discussed by Smith and Woolf [3] to infer rainfall rates. The regression method employs data from eight of the SMMR channels.

Unfortunately, the size of the antenna of the SMMR on Nimbus-7 imposes a diffraction limit on the sensor's angular resolution such that the relative angular response, d, of the radiometer is a function of the channel frequency. The antenna response function can be approximated by the

diffraction pattern of a circularly symmetric aperture with uniform illumination. The normalized radiation pattern, or the response function d, is of the form

$$d(\theta) = \left[\frac{J_1(ka \sin\theta)}{ka \sin\theta}\right]^2 , \qquad (1)$$

where a is the antenna radius, θ is the angular deviation from the antenna centerline, $k = 2\pi/\lambda$ is the wave number and $J_1(\cdot)$ is the first-order Bessel function. SMMR channels at different frequencies therefore have different footprint sizes, where the term footprint, or instantaneous field of view, is the most frequently used definition of the spatial resolution of a satellite radiometer. The foot prints corresponding to the half-power beamwidths of each channel are shown in Table 1. It is difficult to apply the regression algorithm unambiguously to real SMMR data, because each channel measures radiation from a footprint which may contain differing amounts of rain. This study overcomes the diffraction limitation imposed on spatial resolution by means of a constrained iterative restoration algorithm.

SMMR Performance Characteristics

PARAMETER	CHANNEL				
	1	2	3	4	5
WAVELENGTH (CM)	4.54	2.8	1.66	1.36	0.81
FREQUENCY (GHz)	6.6	10.7	18.0	21.0	37.0
DYNAMIC RANGE (° K)	10 - 330				
FOOTPRINT SIZE (KM^2) (PICTURE ELEMENT)	148×95	91×59	55×41	44×30	27×18

Table 1.

II. Iterative Image Restoration - An Introduction

The problem of image degradation can be stated mathematically as follows: the observed image, $b(x,y)$, is expressed as

$$b(x,y) = \ell(x,y) * d(x,y) + n(x,y), \tag{2}$$

where

$d(x,y)$ is the point spread response function of the degradation,

$\ell(x,y)$ is the ideal image,

$n(x,y)$ is random noise, and

$*$ denotes a convolution operator

In the frequency domain, we can also represent the spectrum of the degraded image by

$$B(\omega_x,\omega_y) = L(\omega_x,\omega_y) \cdot D(\omega_x,\omega_y) + N(\omega_x,\omega_y) \tag{3}$$

where B, L, D, N are the Fourier transformations of b, ℓ, d, and n, respectively.

One approach to the image restoration problem is based on the concept of inverse filtering, in which the degradation point spread function is inverted to obtain a restored image. This approach is by solving for either an estimate of the ideal image ℓ or its transform L.

There have been a number of methods developed in recent years to restore degraded images, such as Wiener filtering, parametric estimation filtering, and pseudoinverse spatial restoration; see Andrews and Hunt [4]. Wiener filtering is perhaps the most popular linear restoration method in which the mean square error between the ideal image and the restored image is minimized. Other commonly used restoration methods include the power spectrum

equalization method that sets the power spectrum of a blurred image equal to that of the original image, and the minimum a posteriori density method that uses Bayes theorem to optimize the restoration.

The major task in linear restoration is to invert the degradation equation which is modeled either by a superposition integral or by a vector-space matrix equation. The existence of a unique inverse of the degradation point spread function, d(x,y), is required to derive $\hat{f}(x,y)$ in the presence of noise, n(x,y). If the inverse transformation of d(x,y) does not exist, then the problem is said to be singular. In those cases for which the inverse exists but is not unique, multiple solutions result. However, even if a unique inverse of d exists, it may be ill-conditioned. It can be shown that an arbitrary small perturbation in b can result in a large perturbation in the solution, $\hat{f}$. Namely, the noise n(x,y) will lead to an undesired solution if the inverse of d is ill-conditioned.

For these reasons, an alternative approach that is based upon iterative processing (successive approximations) to image restoration is of interest. This approach has the advantage that it is not necessary to determine the inverse of the point spread function. It has been demonstrated in a number of studies and applications that the sequence of approximations converges to a unique solution if constraints based upon known properties of the desired solution are incorporated into the iterative procedure. The use of iterative methods provides the flexibility of mixing constraints and distortions which is essential in solving many practical restoration problems. It is also evident from past work that this approach may provide a relatively efficient solution for linear spatially varying and nonlinear degradation problems (see Schafer, et al. [8] for a survey of iterative restoration algorithms).

For diffraction-limited imaging, the restoration of the image beyond the diffraction limit cannot be accomplished by filters that are based upon an inversion of convolution equation. The removal of noise and distortion is obtained at the expense of resolution. However, the use of iterative restoration techniques may provide superresolution in the presence of noise. Such techniques make use of an incomplete a priori knowledge that we may have about the original image and the imaging system in order to extrapolate the bandlimited image spectrum beyond its diffraction limit. The incorporation of prior knowledge of the image signal in the restoration process may be considered as a constraint operator which operates on the image signal iteratively to correct for imaging distortions.

An iterative restoration technique using a spectral extrapolation algorithm was developed by Gerchberg [5] for the reconstruction of the signal of an object with a known finite duration or extent. In this method the a priori constraint operates on the signal's magnitude and the magnitude of its Fourier transform. Papoulis [6] proposed the same algorithm assuming a bandlimited signal and emphasizing signal extrapolation. Both of these methods are based on the fact that a finite object has an analytic spectrum. Analyticity implies that knowledge of only part of the spectrum is sufficient to uniquely determine the remainder of the spectrum. Hence, the complete spectrum may be derived from a diffraction-limited image although the information content may be incomplete.

The Gerchberg-Papoulis algorithm has been studied and applied by a number of researchers. Sabri and Steenaart [7] derived a fast bandlimited signal extrapolation method using a matrix formulation. Another similar approach to the extrapolation of a bandlimited signal was proposed by Cadzow [16]. Rushforth and Frost [9] introduced a modified version of the Gerchberg-

Papoulis algorithm that provides additional flexibility and reduces the sensitivity to noise. Youla [10] generalized the algorithm using an alternating orthogonal projection method in Hilbert space and developed general conditions for convergence. Stack, Cahana, and Webb [11] formulated the restoration of finite-energy objects from two projections. Cahana and Stark [12] extended the algorithm to produce a faster convergence rate. Howard [13] formulated the algorithm as the solution of a system of linear equations containing Fourier components. Maeda and Murata [14] attempted to suppress noise in the restoration algorithm by preprocessing the image by a conventional spatial frequency filter. Fienup [15] proposed a version of the iterative algorithm for reconstruction using the magnitude of the Fourier transform of a signal with positivity constraints. More recently, Hayes, Lim, and Oppenheim [17], [18] have investigated iterative procedures for the reconstruction of signals with finite extent from either the phase or the magnitude of the Fourier transform. All of these methods fit into the general framework of a general iterative restoration algorithm, with the Gerchberg-Papoulis algorithm being perhaps the most widely know algorithm of this type.

In the following section, we will discuss the mathematical framework, convergence criteria, and the effect of noise in the general Gerchberg-Papoulis algorithm. Some of the mathematical formalism and notation used by Youla [10] and Stark et al. [11] will be used here to describe the iterative restoration procedure. Experimental results obtained by applying a modified Garchberg-Papoulis algorithm to the restoration of multichannel microwave imagery will be presented.

III. The Constrained Iterative Restoration Algorithm

A. The Resoration Algorithm

Consider the Hilbert space H with elements f, g, h, x, etc., consisting of all L_2 square-integrable, Fourier-transformable functions, with inner product

$$(f,g) = \int_{-\infty}^{\infty} f(x) \cdot g(x)\, dx \tag{4}$$

and norm

$$\|f\| = \left[\int_{-\infty}^{\infty} [f(x)]^2\, dx \right]^{1/2}. \tag{5}$$

Let H_1 and H_2 be two subspaces of H. The angle between the two subspaces is defined by the expression

$$\psi(H_1, H_2) = \cos^{-1} \left(\sup_{\substack{f \in H_1 \\ g \in H_2}} \frac{|(f,g)|}{\|f\| \cdot \|g\|} \right). \tag{6}$$

The angle $\psi=0$ occurs when H_1 and H_2 are orthogonal to each other. For each $f \in H$ we have a unique decomposition

$$f = g + h, \tag{7}$$

where g is the projection of f onto the subspace $\mathcal{P}$ and h is the projection of f onto the orthogonal complement of $\mathcal{P}$, denoted by $\perp \mathcal{P}$. Since g and h are mutually orthogonal, the inner product $(g,h) = 0$.

Two linear operators $P(\cdot)$ and $Q(\cdot)$ are defined by the rules

$$g = P(f) \text{ and } h = Q(f), \tag{8}$$

respectively. P and Q are orthogonal operators which project the function $f \in H$ onto the orthogonal subspaces $\mathcal{P}$ and $\perp \mathcal{P}$, respectively.

Let us associate these two projection operators with the transformation of image signals between the spatial domain and the frequency domain via the Fourier transformation pair. Let $P_a(\cdot)$ and $Q_a(\cdot)$ denote the projection operators in the spatial domain which project onto $\mathcal{P}_a$ and $\perp \mathcal{P}_a$, respectively. Similarly, let $P_b(\cdot)$ and $Q_b(\cdot)$ be the operators in the frequency domain which project onto $\mathcal{P}_b$ and $\perp \mathcal{P}_b$, respectively.

For example, if a portion of the ideal image $f(x)$ is known a priori (say, we have an unknown object in a background of known intensity), the unknown portion of $f(x)$ can be expressed using the spatial projection operator, P_a, as

$$M(x) \cdot f(x) = P_a(f) , \tag{9}$$

while the known portion of the image $f(x)$ is expressed using the projection operator Q_a as

$$(1 - M(x)) \cdot f(x) = Q_a(f) , \tag{10}$$

where

$$M(x) = \begin{cases} 1, & x \in \text{unknown extent} \\ 0, & x \in \text{known extent} . \end{cases}$$

This pair of spatial projection operators decomposes the image signal f into two parts: the unknown portion of the signal $P_a(f)$, and the known portion $Q_a(f)$, where $f = P_a(f) + Q_a(f)$ and $(P_a(f), Q_a(f)) = 0$.

By dividing the image spectrum into two spectral bands at ω_c, that is, a low-pass spectrum with $|\omega| < \omega_c$ and a high-pass spectrum with $|\omega| \geq \omega_c$, the image signal f is decomposed by two projections $f = P_b(f) + Q_b(f)$ with $(P_b(f), Q_b(f)) = 0$. The operators $P_b(\cdot)$ and $Q_b(\cdot)$ are defined by the following equations:

$$\mathcal{F}^{-1}[M(\omega) \cdot F(\omega)] = P_b(f) \tag{11}$$

$$\mathcal{F}^{-1}[(1 - M(\omega)) \cdot F(\omega)] = Q_b(f), \tag{12}$$

where

$F(\omega)$ is the Fourier transform of $f(x)$,

$\mathcal{F}^{-1}[\cdot]$ denotes inverse Fourier transformation,

P_b and Q_b are projection operators onto the low-pass and high-pass image subspaces, respectively, and

$$M(\omega) = \begin{cases} 1, & \text{for } |\omega| < \omega_c \\ 0, & \text{for } |\omega| \geq \omega_c. \end{cases}$$

The iterative image restoration problem can be stated as follows: given the projections of the image signal on prescribed subspaces, can one derive the original image $f(x)$? It has been proved by Stark, et al. [11] that the restoration is possible under certain conditions if partial information from the subspaces is given.

To be more precise, let us consider an example: If we are given two projections of $f(x)$, say $g = Q_a(f)$ and $h = P_b(f)$ as defined in (10) and (11), respectively, then a restoration is possible. In this case, $g = Q_a(f)$ is considered to be the portion of the image data which vanishes outside some known extent, and $h = P_b(f)$ is considered to be the low-pass signal of a bandlimited image. The low-pass spectrum, $\mathcal{F}[P_b(f)]$, is the truncated spectrum of the image f. This low-pass spectrum can be obtained from the fact that the low-frequency components of the degraded image have not been changed, or the knowledge of the degradation function is known. This example is equivalent to the extrapolation problem described by Gerchberg [5] and by Papoulis [6].

Before starting the iterative restoration algorithm, we first define the notation of iterative projection, $(P_a Q_b)^{(k)}(f)$, explicitly by

$$(P_a Q_b)^{(k)}(f) = P_a(Q_b(P_a(Q_b(P_a \ldots P_a(Q_b(f)))))\ldots), \tag{13}$$

where both P_a and Q_b operate k times. For example,

$$\begin{aligned} (P_a Q_b)^{(0)}(f) &= f \\ (P_a Q_b)^{(1)}(f) &= P_a(Q_b(f)) \\ (P_a Q_b)^{(2)}(f) &= P_a(Q_b(P_a(Q_b(f)))) \ . \end{aligned} \tag{14}$$

Then, the iterative method is stated as follows:

Step 1: Obtain the signal $P_b(f)$ and $Q_a(f)$, based on available a priori information.

Step 2: Let k=1, and let the first guess of the iteration process be

$$f^{(1)} = P_a(P_b(f)) + Q_a(f). \tag{15}$$

Note that $f^{(k)}$ is the enhanced image after k-1 iterations.

Step 3: Correct the error by imposing constraints in the spectral domain.

$$f' = f^{(k)} - P_b(f^{(k)}) + P_b(f) \tag{16}$$

Step 4: Correct the error by imposing constraints in the spatial domain,

$$f^{(k+1)} = f' - Q_a(f') + Q_a(f) \tag{17}$$

Step 5: Let k = k + 1. If a satisfying result is obtained, stop. Otherwise, go to step 3.

Figure 1 shows the block diagram of the restoration method.

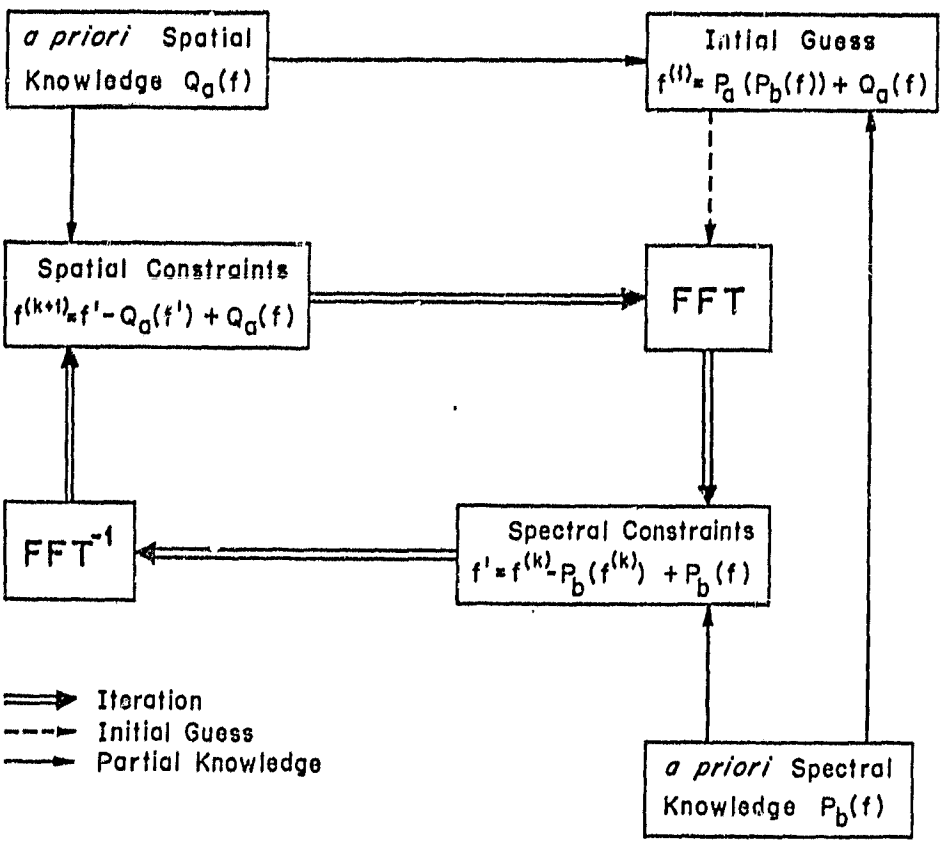

Figure 1. Block Diagram of the Constrained Iterative Restoration Algorithm.

The procedure begins with an initial guess as in (15) by performing the operation P_a on the signal $P_b(f)$ to remove all the signal from regions where *a priori* data are available. Adding $Q_a(f)$ then restores the correct values back into those regions. Both the correct values and their corresponding spatial locations are assumed to be known. This initial guess, $f^{(1)}$, is the result of a one-step Gerchberg-Papoulis algorithm, which performs error correction on the low-pass filtered image, $P_b(f)$, using incomplete information.

In step 3, spectral constraints are imposed according to (16) where incorrect low frequency components at the k^{th} iteration, $P_b(f^{(k)})$, are replaced with spectral information $P_b(f)$ that is assumed to be known. In step 4, spatial constraints are imposed according to (17); the resulting signal f' from (16) is corrected by removing $Q_a(f')$ and replaced by the known spatial information $Q_a(f)$.

It is easy to show that Equations (16) and (17) are functions of $f^{(k-1)}$, the previous iteration result, and $f^{(1)}$, the initial guess as in Eq. (15). Substituting Eq. (16) into Eq. (17), and letting k = 2,3,..., we obtain

$$\begin{aligned} f^{(2)} &= P_a(Q_b(f^{(1)})) + f^{(1)} \\ f^{(3)} &= P_a(Q_b(f^{(2)})) + f^{(1)} \\ &\vdots \qquad\qquad\qquad \vdots \\ f^{(k)} &= P_a(Q_b(f^{(k-1)})) + f^{(1)} \end{aligned} \tag{18}$$

Solving these equations recursively, a simple equation is obtained for the k^{th} image iterate:

$$f^{(k)} = \sum_{j=0}^{k-1} (P_a Q_b)^{(j)}(f - (P_a Q_b)(f))$$
$$= f - (P_a Q_b)^{(k)}(f) \tag{19}$$

The reconstructed image $f^{(k)}$ can thus be considered as the difference between the ideal image f and the k-times projected version of the ideal image, $(P_a Q_b)^{(k)}(f)$. In other words, $f^{(k)}$ depends on the ideal image function f, the projection operation $P_a Q_b$, and the number of iterations. If $f^{(k)}$ is an estimate of f, then $e^{(k)} = (P_a Q_b)^{(k)}(f)$ is the error in the k^{th} image iterate.

Since Q_b and P_a are projection operators, the norm (or power) of the projection onto the subspace is less than or equal to that of the mapping signal, that is,

$$\|f\| \geq \|Q_b(f)\|,$$
$$\|f\| \geq \|P_a(f)\|, \text{ and} \tag{20}$$
$$\|f\| \geq \|(P_a Q_b)(f)\| .$$

The error term in the $(k+1)^{st}$ iterate, $e^{(k+1)}$, can be expressed in terms of $e^{(k)}$, the error in the k^{th} iterate by

$$e^{(k+1)} = (P_a Q_b)^{(k+1)}(f) \tag{21}$$
$$= P_a Q_b((P_a Q_b)^{(k)}(f))$$
$$= (P_a Q_b)(e^{(k)}),$$

with

$$\|e^{(k+1)}\| \leq \|(P_a Q_b)(e^{(k)})\| . \tag{22}$$

This implies that the error is strictly monotonically decreasing, and it has been proved [10] that recursion Eq. (19) converges to f as k approaches infinity, if and only if $\mathcal{P}_a \cap \perp \mathcal{P}_b = \{\ \}$ and $\psi(\mathcal{P}_a, \perp \mathcal{P}_b) > 0$.

In practical situations the iterative process converges to some constant not equal to f for some finite k, in which $(P_aQ_b)^{(k)}(f) \cong (P_aQ_b)^{(k+1)}(f)$. This is mainly due to noise generated by imaging, quantization error, an inaccurate estimate of the degradation function, etc. One important noise source that will further affect the performance of the restoration is the insufficiency of a priori constraints. In this situation the prescribed subspaces do not provide sufficient information for the restoration when $\psi(\mathcal{P}_a, \perp \mathcal{P}_b)$ is very small. Such a situation can be improved by incorporating more constraints into the procedure.

B. Restoration with Noisy Constraints

Insufficient or inaccurate constraints imposed on the restoration procedure will lead to undesirable results even if the iteration process converges. For example, if we have some uncertainties in the projection operators which project onto subspaces $\mathcal{P}$ and $\perp \mathcal{P}$, the extrapolated signal will inevitably contain some error, and this error will amplify in the iteration process. In most cases, noisy constraints are the result of wrong assumptions in the physical model of the problem, or from noisy image signals used to constrain the data.

We now demonstrate the effect of noisy constraints on image resolution restoration. We use two projections of f(x), say g' and h', where $g' = (Q_a(f) + n_s)$ and $h' = (P_b(f) + n_f)$, to represent the amount of additive noise embedded in the partial information from the two prescribed subspaces. In the case of bandlimited image extrapolation, n_s and n_f represent erroneous

constraints in the spatial and frequency domains, respectivly. The initial guess $f^{(1)}$ of the iterative procedure becomes

$$f^{(1)} = P_a(P_b(f) + n_f) + (Q_a(f) + n_s). \tag{23}$$

By substituting $f = P_a(f) + Q_a(f)$ and $f = P_b(f) + Q_b(f)$ into (23), we have

$$\begin{aligned} f^{(1)} &= P_a(P_b(f)) + f - P_a(f) + P_a(n_f) + n_s \qquad (24) \\ &= [f - P_a(Q_b(f))] + [P_a(n_f) + n_s]. \end{aligned}$$

Rewriting (16) and (17) using the noisy constraints, we obtained the recursion formula

$$\begin{aligned} f^{(k)} &= \sum_{j=0}^{k-1} (P_aQ_b)^{(j)}(f - P_a(Q_b(f)) + P_a(n_f) + n_s) \qquad (25) \\ &= f - (P_aQ_b)^{(k)}(f) + \sum_{j=0}^{k-1} (P_aQ_b)^{(j)}(P_a(n_f) + n_s) \\ &= f - e^{(k)}. \end{aligned}$$

The error $e^{(k)}$ in the restored image $f^{(k)}$ consists of two terms. The first term $(P_aQ_b)^{(k)}(f)$ decreases monotonically while the second term $\sum_{j}^{k-1} (P_aQ_b)^{(j)}(P_a(n_f) + n_s)$ increases monotonically as the number of iterations k increases. One must therefore consider the tradeoff between these two error terms in deciding how many iterations should be applied. If the image signal is much stronger than the noise signal, the iterative procedure will converge within a reasonable number of iterations. For the case of extremely noisy constraints, the second error term becomes dominant. Thus, fewer iterations will provide satisfying results while more iterations will lead to divergence.

In one experiment a square object in a square background field, both with constant signal levels, was used to demonstrate the tradeoff between performance and the number of iterations. The test image was first degraded

by a low-pass filter. The bandlimited image was then restored by the above-described constrained iterative algorithm. The cutoff frequency of the image signal was assumed to be known and it was used as a constraint in the frequency domain. The physical extent of the square object and the signal from the background were considered as partial a priori spatial information. To generate the effects of noisy constraints, independent noise was added to the spatial constraint. This was done by corrupting the signal of the background with additive zero-mean white Gaussian noise. Noise levels with different standard deviations (0, 5, 10, 20, 30, and 40) were used. The restored images were evaluated by measuring the mean-square error between the ideal image and the restored image. Figure 2 shows the resultant curves representing the performance of the algorithm at different noise levels. At low noise levels, the procedure converges in a reasonable number of iterations to a low error rate. This implies that the bandlimited image has been successfully restored. With higher noise levels in the constrained data, the second term of $e^{(k)}$ in (25) becomes dominant and the algorithm performance deteriorates as k increases. This experiment confirms that the restoration results are sensitive to the number of iterations when noisy constraints are used.

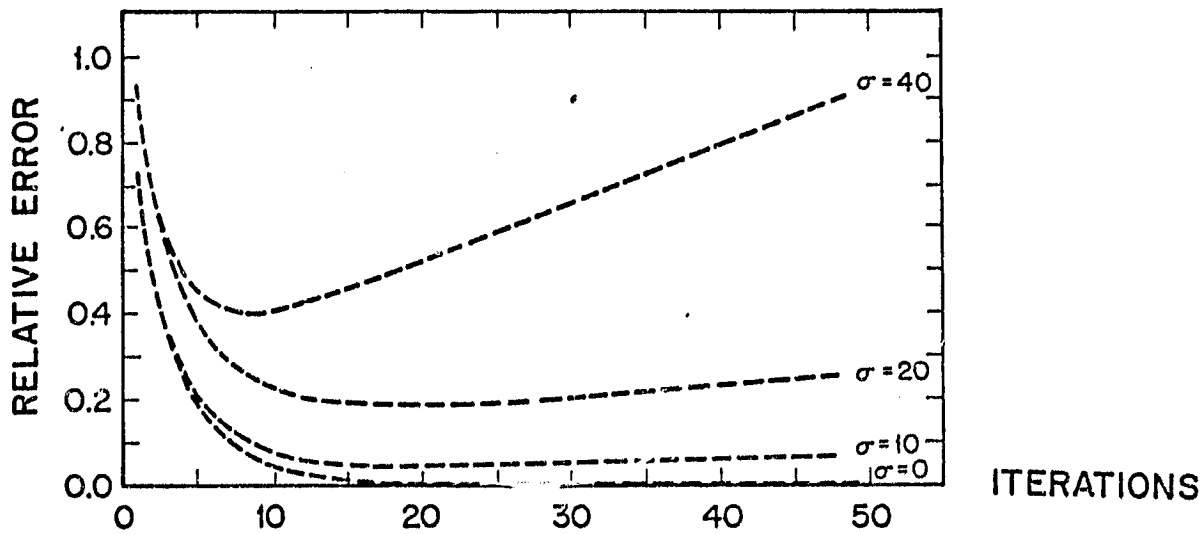

Figure 2. Performance of the algorithm with noisy constraints at different noise levels.

IV. Restoration of Multichannel Microwave Images

The image restoration procedure described above has been aplied to overcome the diffraction-limited imagery obtained from the SMMR. The goal is to restore channels of low spatial resolution to a common high resolution. The low frequency bandlimited images are obtained from the 21.0, 18.0, 10.7, and 6.6 GHz channels, and the common high resolution is that of the 37 GHz channels.

The procedure described in Section III was implemented with special features, which accommodates the multichannel SMMR imagery of hurricanes. The procedure is summarized in Figure 3. Details of the partial constraints will be discussed in the following sections.

A. Spatial Constraints, $Q_a(f)$

Spatial constraints are based on the estimated extent of rain areas, derived from the 37 GHz and infrared images, the upper and lower bounds of the measured brightness temperatures, and some physical attributes of hurricanes.

We initially utilized polarization information at 37 GHz to provide an *a priori* estimate of the spatial extent of model hurricane raincells. While microwave emission from the ocean surface is highly polarized, the emission from raincells is nearly unpolarized. Therefore, a polarization threshold was applied to the 37 GHz antenna temperatures to identify areas of significant rainfall (rainfall rate $\gtrsim$ 2 mm/hour).

A simple physical model was then employed to relate the 37 GHz antenna temperatures outside the rain areas to antenna temperatures at the lower microwave frequencies. In these regions, the microwave antenna temperature, T_B, at frequency ν and in polarization p can be expressed as

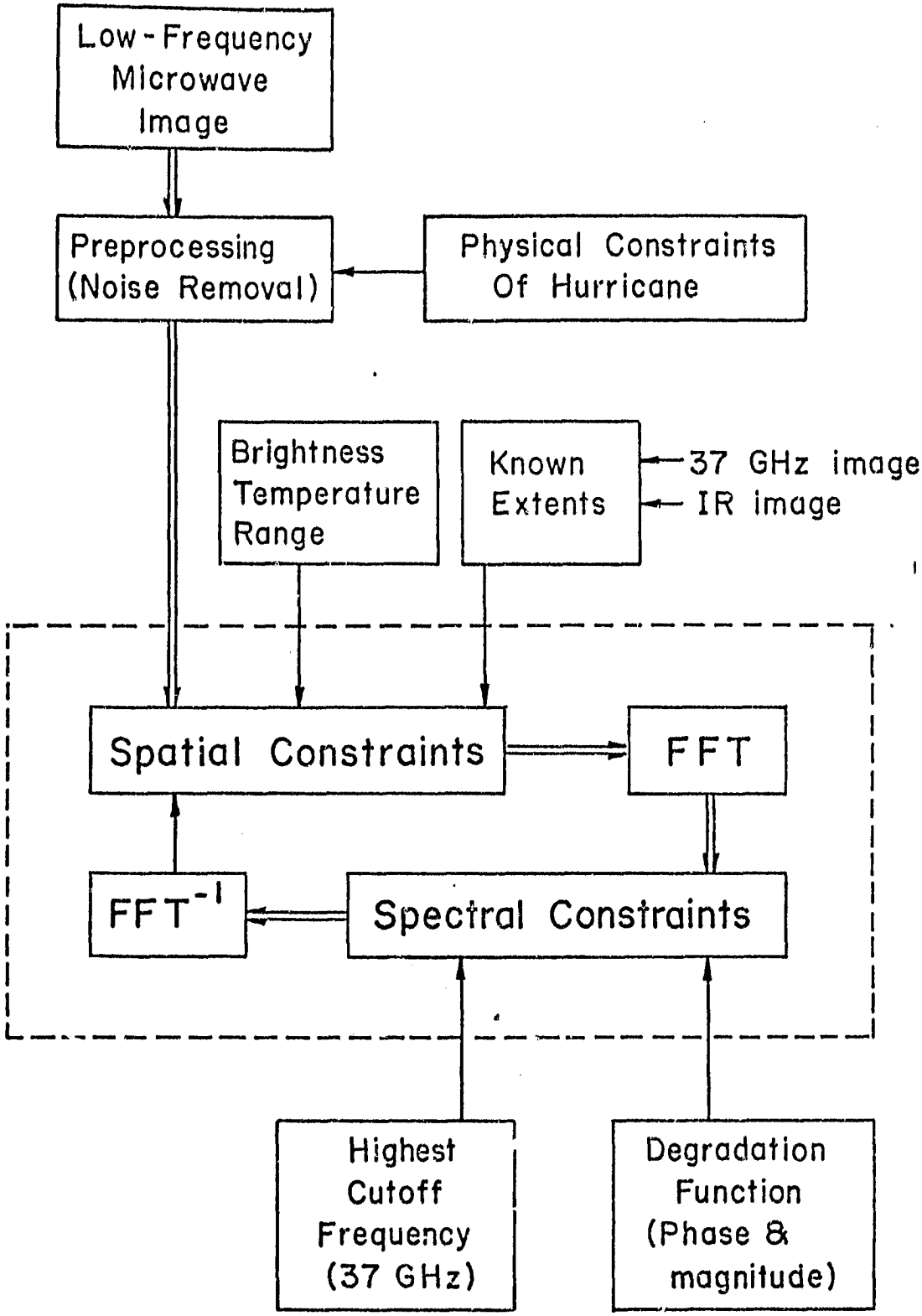

Figure 3. The procedure to restore low frequency SMMR images (6.6, 10.7, and 18.0 GHz) to a high common resolution (that of the 37 GHz channels).

$$T_B(\nu, p) = (1 - r(\nu, p)) \cdot T_{IR}\, \Pi(\nu) \qquad (21)$$

$$+ T_A(\nu) \cdot (1 - \Pi(\nu)) \cdot (1 + r(\nu,p) \cdot \Pi(\nu))$$

$$+ T_{bb} \cdot \Pi^2(\nu) \cdot r(\nu,p),$$

where $$T_A(\nu) = T_1(\nu) + T_2(\nu) \cdot (1 - \Pi(\nu))$$

is the effective emitting temperature of the atmosphere. $T_{bb} = 2.7\ ^0K$ is the cosmic microwave background, and T_{IR} is the infrared ocean surface temperature, which can be obtained operationally from geostationary satellites. The constants $T_1(\nu)$ and $T_2(\nu)$ are obtained empirically. The atmospheric transmittance is $\Pi(\nu)$, and the ocean surface reflectivity, $r(\nu,p)$, can be expressed [19]

$$r(\nu, p) = \alpha(\nu, p) - \beta(\nu) \cdot U_{20}, \qquad (22)$$

where U_{20} is the wind speed at 20 m height, and $\alpha(\nu, p)$ and $\beta(\nu)$ are empirical constants. The three terms on the right-hand side of (21) represent surface emission, atmospheric emission, and the small contribution from the cosmic background, respectively.

From (21) and (22) it may be noted that each antenna temperature depends only upon the two unknown quantities $\Pi(\nu)$ and U_{20}. Thus, antenna temperature measurements in the two polarizations at 37 GHz provide enough information to solve simultaneoulsy for Π(37 GHz) and U_{20}. Since the transmittance at 37 GHz is related empirically to transmittances at the lower frequency channels, T_B (21.0, p), T_B (18.0, p), T_B (10.7, p) and T_B (6.6, p) can also be computed.

In areas where the rainfall rate did not exceed ~ 2mm/hour the above method (Eqs. (21) and (22)) was utilized to recreate imagery in the low frequency channels with 37 GHz resolution. This "known" portion of each low

frequency image was then used as a partial constraint, or incomplete information, to extend the resolution in the heavier rain areas.

B. Spectral Constraints, $P_b(f)$

The spectral constraints used in the restoration algorithm are based on a knowledge of the highest cutoff frequency (defined by the 37 GHz resolution), and a knowledge of the degradation point spread function. The SMMR antenna aperture illumination function is considered to be the degradation point spread function of the imaging process.

In this initial study, a Bessel-type point spread function was used to describe the passive microwave radiometer response; see Eq. (1). This response function is a simplified model of the actual SMMR antenna aperture illumination that allows us to assume a flat response function at the low frequency portion of the spectrum. During the iteration, the DC and a few low frequency components (both the phase and amplitude) of the image spectrum were kept intact, while frequency components above 37 GHz were removed.

This simple response function (1), with the assumption of a uniformly illuminated aperture, does not agree in general with the actual SMMR antenna aperture illumination function for which one must assume non-uniform distribution. In order to apply the restoration algorithm to real microwave image data, a more realistic degradation point spread function will be needed.

One can empirically estimate the amplitude and phase distribution functions of the SMMR instrument. One can also model the antenna response through analytical methods. The most commonly used phase distributions across the aperture are linear and quadratic functions, where linear-phase illumination is the basic principle behind an electronic scanning antenna, and quadratic-phase illumination functions are used primarily to effect far-field

conditions in the Fresnal region of the diffracted field. The amplitude illumination is governed by antenna parameters such as the antenna directivity, the side-lobe energy level, and the half-power beamwidth. The amplitude illumination function of a particular antenna can be modeled by matching the antenna parameters with those produced by selected distribution functions, such as the cosine functions, the parabolic functions, etc.

Given an estimate of the point spread function -- both in phase and amplitude -- we will be able to constrain the spectrum during the iterative restoration process and apply the procedure to restore the 6.6, 10.7, 18.0, and 21.0 GHz SMMR channels to a common, high resolution (that of the 37 GHz channels).

C. Experiments and Results

A set of synthetic hurricane images, each consisting of antenna temperatures in a 16 × 16 pixel image field, were created. Noise-free antenna temperatures at 37.0, 18.0, 10.7, and 6.6 GHz were generated using the approximate radiative transfer model of Olson [1], assuming an ocean surface background (see Figure 4). After the restoration, the low frequency channels were enhanced to a resolution compatible with the 37 GHz channel. The enhanced images are shown in Figure 5.

Figure 6a shows the cross-sections of rain cells in the 6.6 GHz synthetic hurricane image before and after restoration. The degraded 6.6 GHz image resolution has been enhanced to a large degree after a few iterations. A synthetic image of the entire model hurricane that would be measured at 37 GHz, the original degraded 6.6 GHz image, and the enhanced 6.6 GHz model hurricane image are shown in Figs. 6b, 6c and 6d respectively.

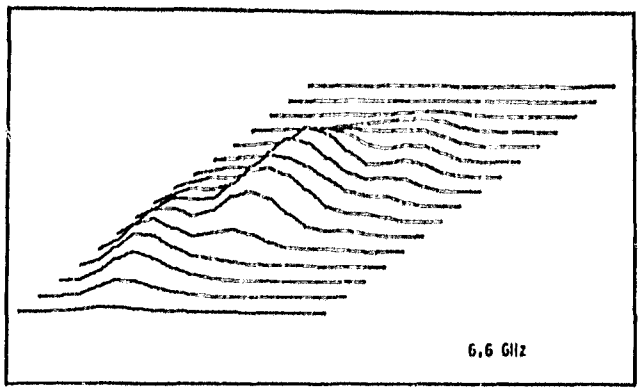

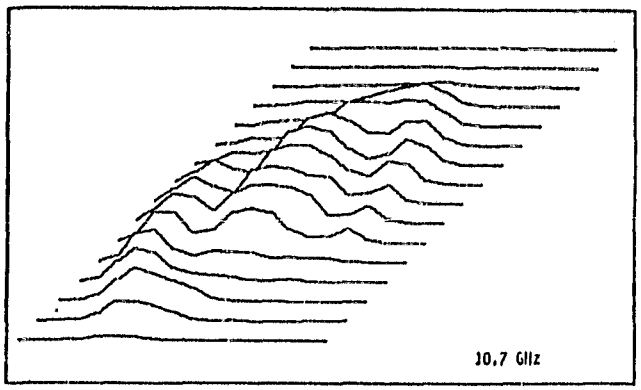

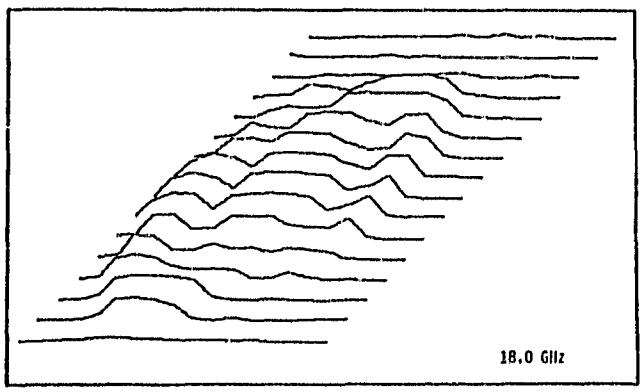

Figure 4. The observed 6.6, 10.7, and 18.0 GHz images at the parallel polarization.

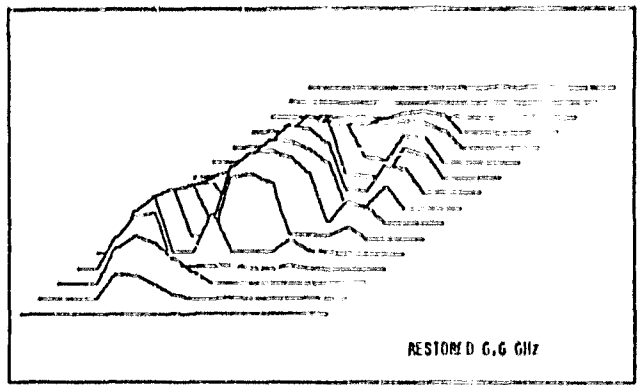

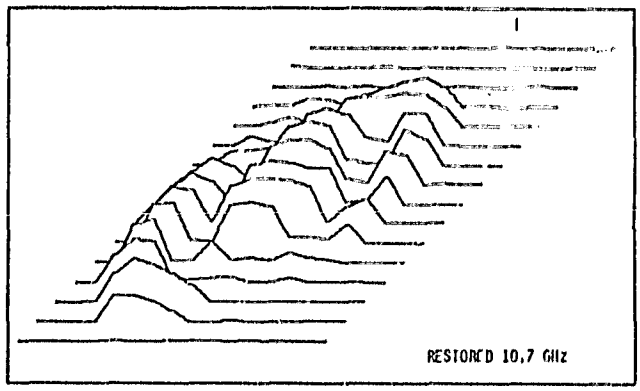

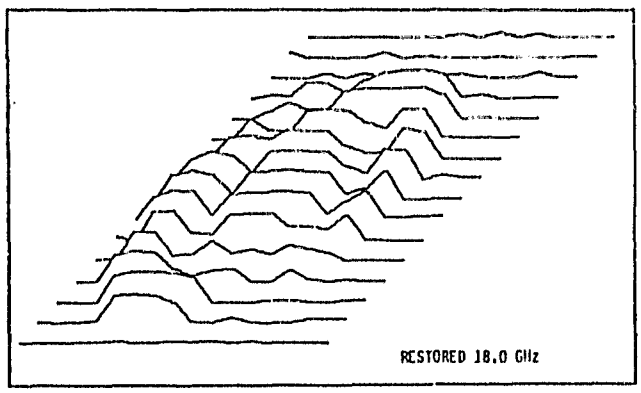

Figure 5. The enhanced 6.6, 10.7, and 18.0 GHz images after 15 iteratons.

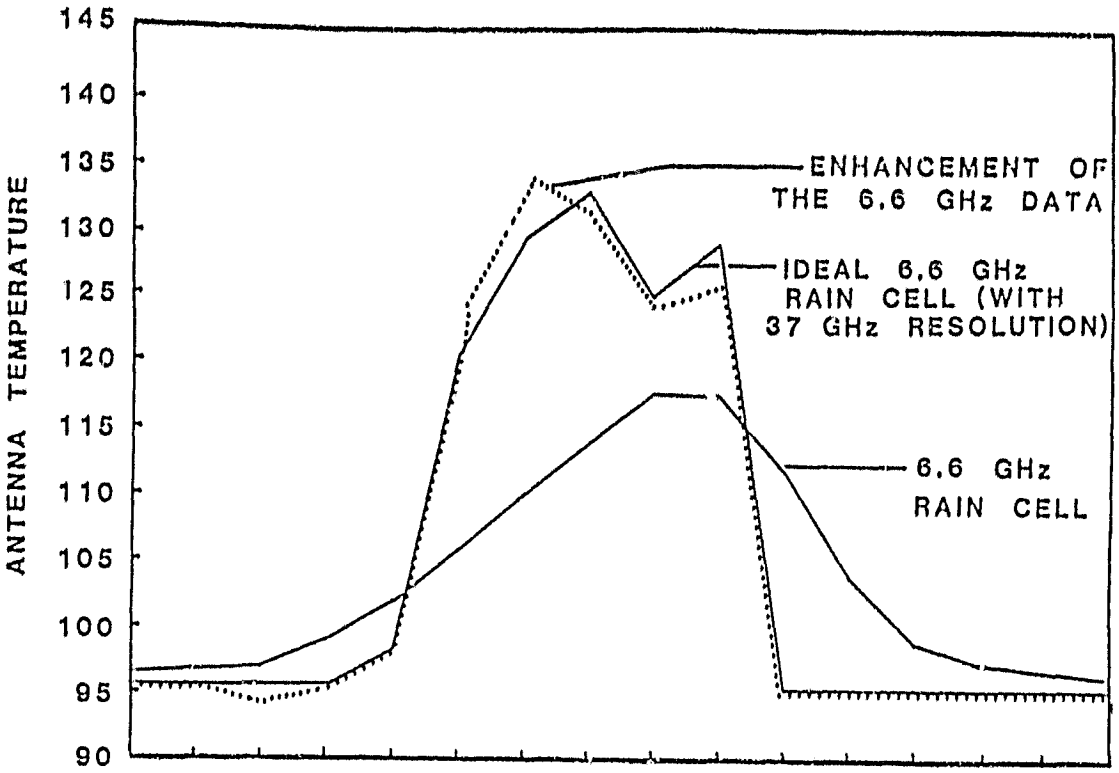

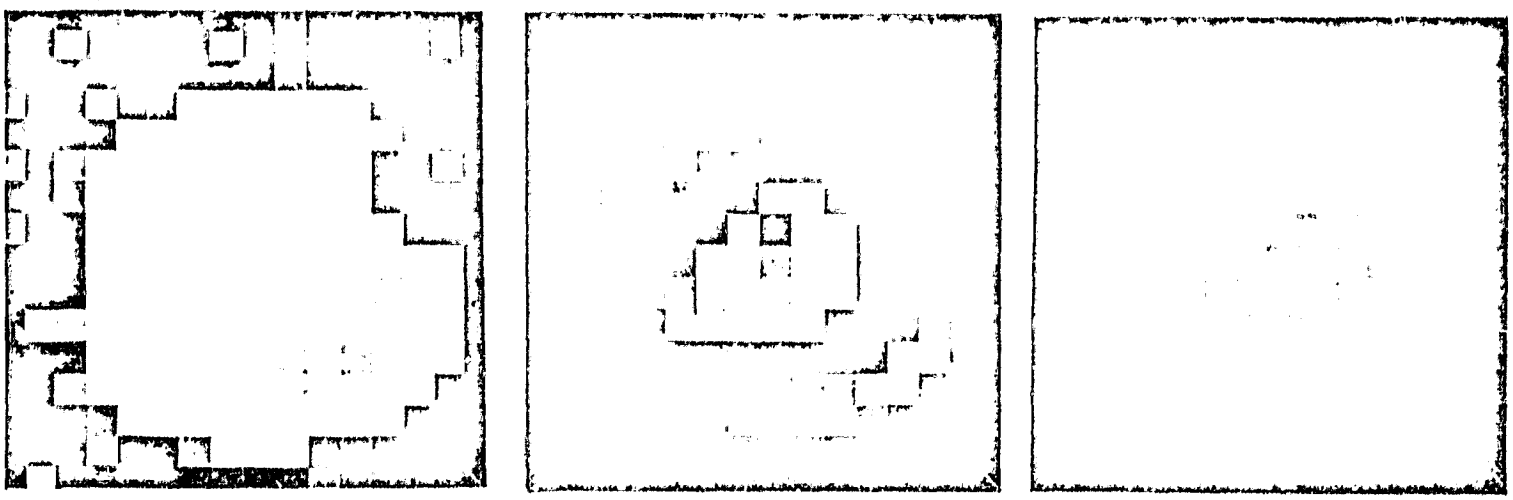

Figure 6. Enhancement of the resolution of a synthetic 6.6 GHz image of a hurricane. A detailed cross-section plot is shown in (a). This enhancement algorithm uses the known extent of the image shown in (b) to enhance the degraded 6.6 GHz image shown in (d). The derived image at 37 GHz resolution is shown in (c).

Data distorted by noise has rendered it difficult to continue the spectrum beyond the original diffraction limitation. The restoration procedure was applied to a set of noisy images to determine its ability to handle noisy data. In one example, additive white noise with an rms value of 4° K was added to both the 37 GHz and 6.6 GHz synthetic images. Within a few iterations, we obtained the restored image scan as shown in Fig. 7. The 6.6 GHz noisy image is almost completely restored to the optimal resolution.

V. Conclusions

An iterative resolution restoration method for restoring multichannel diffraction-limited imagery has been described. It is based upon the Gerchberg-Papoulis algorithm using incomplete information and partial constraints in both the image space and the Fourier space. The procedure was presented using the orthogonal projection formulation proposed by Youla [10] where projection operators project onto two prescribed subspaces. The projection operators are defined by incorporating a priori information of the imaging system and the nature of the observed object. The tradeoff between error and convergence rates has also been investigated.

One of the focuses of this research was on the multichannel microwave image restoration problem, with special attention paid to the selection of appropriate constraints for the iteration procedure. It was demonstrated that the constraints control the performance and rate of convergence of the restoration. Using the procedure, a set of synthetic hurricane images was restored to a common resolution.

This application has shown the effectiveness of this iterative procedure in restoring the spatial resolution of low frequency channels. An obvious next step is to apply this procedure to real multichannel data.

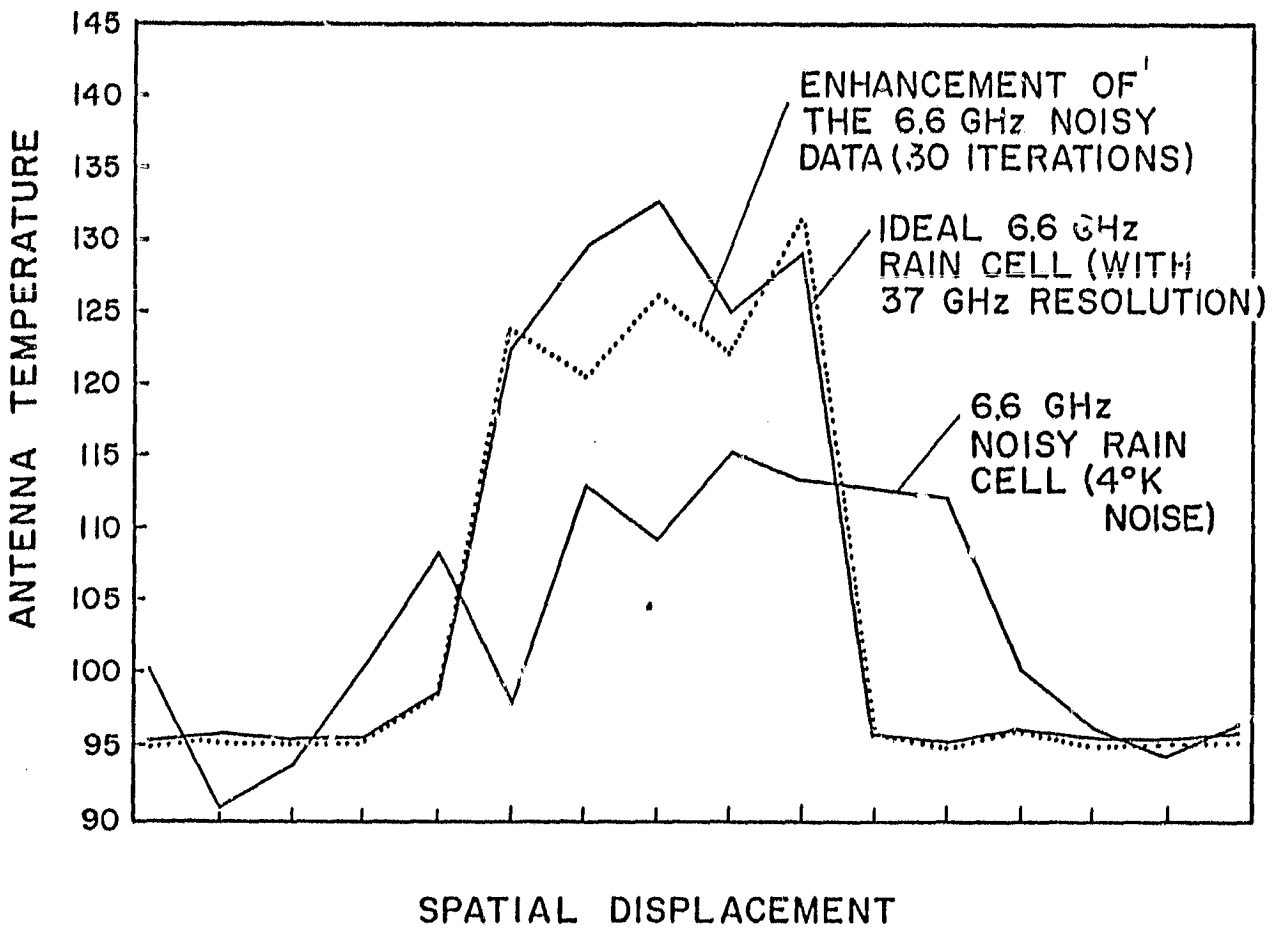

Figure 7. Restoration of Noisy Images.

References

[1] Wilheit, T. T., A. T. C. Chang, M. S. V. Rao, E. B. Rodgers, J. S. Theon, "A Satellite Technique for Quantitatively Mapping Rainfall Rates Over the Ocean," J. Appl. Meteo., 16, pp. 551-560, 1977.

[2] Olson, W. S., "Estimation of Rainfall Rates in Tropical Cyclones by Passive Microwave Radiometry," Ph.D. thesis, Department of Meteorology, University of Wisconsin-Madison, 1983.

[3] Smith, W. L. and H. M Woolf, "The Use of Eigenvectors of Statistical Covariance Matrices for Interpreting Satellite Sounding Radiometer Observations," J. Atms. Sci., 33, pp. 1127-1140, 1976.

[4] Andrews, H. C. and B. R. Hunt, Digital Image Restoration, Prentice-Hall, Inc., 1977.

[5] Gerchberg, R. W., "Super-Resolution Through Error Energy Reduction," Optica Acta, 21, 709-720 (1974).

[6] Papoulis, A., "A New Algorithm in Spectral Analysis and Bandlimited Extrapolation," IEEE Trans. Circuits and Systems, CAS-22(9), 735-742 1975.

[7] Sabri, M. S. and W. Steenaart, "An Approach to Bandlimited Signal Extrapolation: The Extrapolation Matrix," IEEE Trans. Circutis and Systems, CAS-25, pp. 74-78, Feb. 1978.

[8] Schafer, R. W., R. M. Mersereau, and M. A. Richards, "Constrained Iterative Restoration Algorithms," Proc. IEEE, 69(4), 432-450, April (1981).

[9] Rushforth, C. K. and R. L. Frost, "Comparison of some Algorithms for Reconstructing Space-Limited Images," J. Opt. Soc. Am., Vol. 70, Nol 12, pp. 1539-1544, Dec. 1980.

[10] Youla, D. C., "Generalized Image Restoration by the Method of Alternating Orthogonal Projections," IEEE trans. Circuits and Systems, CAS-25(9), 694-702, September 1978.

[11] Stark, H., D. Cahana, and H. Webb, "Restoration of Arbitrary Finite-Energy Optical Objects from Limited Spatial and Spectral Information," J. Opt. Soc. Am., 71(6), 635-642, June 1981.

[12] Cahana, D., and H. Stark, "Bandlimited Image Extrapolation with Faster Convergence," Applied Optics, Vol. 20, No. 16, pp. 2780-2786, August 1981.

[13] Howard, S. J., "Method for Continuing Fourier Spectra Given by the Fast Fourier Transform," J. Opt. Soc. Am., 71, 95-98 1981.

[14] Maeda, J. and K. Murata, "Digital Restoration of Incoherent Bandlimited Images," Applied Optics, Vol. 21, No. 12, pp. 2199-2204, June 1982.

[15] Fienup, J. R., "Reconstruction of an Object from the Modulus of its Fourier Transform," Opt. Letters, Vol. 3, No. 1, pp. 27-29, July 1978.

[16] Cadzow, J. A., "An Extrapolation Procedure for Band-Limited Signals," IEEE Trans. Acoust., Speech, Signal Processing, Vol. ASSP-27, pp. 4-12, Feb. 1979.

[17] Oppenheim, A. V. and J. S. Lim, "The Importance of Phase in Signal," Proc. of IEEE, Vol. 69, No. 5, pp. 529-541, May 1981.

[18] Hayes, M. H., J. S. Lim, and A. V. Oppenheim, "Iterative Techniques for Minimum Phase Signal Reconstruction from Phase or Magnitude," IEEE Trans. Acoust., Speech, Signal Processing, Vol. ASSP-28, pp. 672-680, Dec. 1980.

[19] Wilheit, T. T., "A Model for the Microwave Emissivity of the Ocean's Surface as a Function of Wind Speed," NASA Technical Memorandum-80278, NASA/GSFC, Greenbelt, MD, 1979.